Enzyme-like Kinetics of Ferryloxy Myoglobin Formation in Films on Electrodes in Microemulsions

Peterson M. Guto[†] and James F. Rusling*[,†,§]

Department of Chemistry, University of Connecticut, Storrs, Connecticut 06269-3060, and Department of Pharmacology, University of Connecticut Health Center, Farmington, Connecticut 06032

Received: August 16, 2005; In Final Form: October 25, 2005

Covalently linked films of the ferric heme protein myoglobin and poly-L-lysine on pyrolytic graphite electrodes reacted with *tert*-butylhydroperoxide (*t*BuOOH) to form ferryloxy protein species according to Michaelis−Menten enzyme kinetics. Rotating disk voltammetry data obtained in microemulsions, micellar solution, and buffers revealed a strong influence of water phase acidity on kinetic parameters. Microemulsion and surfactant type had a much smaller influence on reaction kinetics, possibly because the reaction takes place entirely in a water environment surrounding Mb in the films in all fluids. A large apparent Michaelis k_{cat} in microemulsions with neutral water phases was offset by much weaker binding as shown by larger protein−substrate dissociation constants (K_m). Acidic SDS microemulsions and pH 2 buffer provided the most efficient reaction conditions as judged by the ratio k_{cat}/K_m. Apparent kinetic constants are most likely governed by acidity-controlled protein conformations and their binding with *t*BuOOH in the intermediate protein−substrate complex.

Introduction

Microemulsions are less expensive, less-toxic alternatives to organic solvents that can provide unique pathway control in electrochemical synthesis.[1−3] These clear, stable nanoheterogeneous fluids are made from oil, water, and surfactants, and sometimes cosurfactants. They are good solvents for both polar and nonpolar reactants.[4] Cosurfactants are often medium chain alcohols that tune interfacial tension and curvature at oil/water interfaces.[4,5] We have developed catalytic electrodes for synthesis in microemulsions using metallopolyion films covalently bound to electrodes to achieve the stability required in these fluids.[6−8]

Biocatalysis promises to have a major impact on future industrial synthetic routes, e.g., in drug syntheses where chirality is important.[9] For this reason, we began to explore films of metalloproteins as catalysts in microemulsions. We hope to combine inexpensive, stable, reusable protein films to provide synthetic selectivity and specificity characteristic of enzymes with the pathway control and reactant solubilization accessible with microemulsions. We recently found that myoglobin (Mb) coadsorbed with surfactant onto carbon electrodes from microemulsions supported efficient catalytic reduction of organohalides consistent with Michaelis−Menten enzyme kinetics.[10] The microemulsions could be used to tune catalytic reactivity according to the hydrophobicity of the reactants. However, this system required the presence of myoglobin in solution to stabilize the adsorbed biocatalyst. More recently, we made films that are more stable in microemulsions by covalently attaching myoglobin onto poly-L-lysine which had been covalently bound to graphite electrodes.[11] We utilized these films to catalyze styrene epoxidation with turnover rates controlled by microemulsion composition that in turn controlled mass transport and reaction site polarity.[12]

While myoglobin (Mb) is predominantly an oxygen transport protein,[13] it also catalyzes peroxide-initiated hydrocarbon oxidations.[14−19] Hydrogen peroxide reacts with ferric Mb to yield intermediate ferryloxy radicals ($^{\bullet}MbFe^{IV}{=}O$) that oxidize substrates by oxygen transfer, e.g., converting styrene to styrene oxide. $^{\bullet}MbFe^{IV}{=}O$ is a transient species with a half-life of about 30 s in neutral pH buffers at room temperature.[20−22] Ferryloxy Mb has been confirmed by Raman, X-ray absorption, Mossbauer, and NMR spectroscopy.[23−25]

Addition of hydrogen peroxide to solution causes a catalytic current at thin Mb film electrodes that is partly due to reduction of the $^{\bullet}MbFe^{IV}{=}O$ formed, but complicated by additional catalytic cycles involving generation of oxygen that contribute to the current.[26] Furthermore, hydrogen peroxide itself can be involved in secondary reactions including protein degradation.

Reduction of *tert*-butylhydroperoxide (*t*BuOOH) by ferric myoglobin produces *tert*-butyl alcohol and $^{\bullet}MbFe^{IV}{=}O$ in a heterolytic peroxide cleavage mechanism.[27−29] A competing homolytic alkylperoxide cleavage mechanism yields alkoxy radicals and nonradical $MbFe^{IV}{=}O$. For metmyoglobin, the homolytic/heterolytic product ratio[27] was ∼0.53, so that ∼67% of products are obtained by the heterolytic pathway. While peroxy and alkoxy radicals could combine to yield oxygen, reported results for this reaction are consistent with low oxygen generation or exchange.[27,28] The heterolytic product butyl alcohol is electroinactive, and competing electrochemical catalytic cycles in the alkylperoxide-induced generation of $^{\bullet}MbFe^{IV}{=}O$ are minimal compared to generation by hydrogen peroxide. Thus, in this work, we employ *t*BuOOH to investigate the kinetics of ferryloxy Mb radical formation in the hope of largely avoiding side reactions that produce electroactive products. The goal of our work is to understand the influence of microemulsion composition on the formation kinetics of this key ferryloxy oxidant. Results reported herein using rotating disk voltammetry show that ferryloxy generation in Mb films follows Michaelis−Menten kinetics and reveal how microemulsion composition,

* Address correspondence to this author. E-mail: james.rusling@uconn.edu.
† University of Connecticut.
§ University of Connecticut Health Center.

10.1021/jp054621w CCC: $30.25
Published on Web 12/03/2005

TABLE 1: Microemulsions (mEs) Used in This Work[a]

type	components	composition	κ, $M\Omega^{-1}$	η, cP
BC	CTAB/pentanol/tetradecane/H_2O	17.5/35/12.5/35	1.6	14.8
BC	SDS/pentanol/tetradecane/0.1 M NaCl	13.3/26.7/8/52	6.0	12.5
O/W	CTAB/butanol/hexadecane/H_2O	5/5.4/1/88	4.2	5.4
O/W	SDS/pentanol/dodecane/0.1 M NaCl	3.35/6.65/1.0/89	10.5	5.4

[a] Acronyms: CTAB = cetyltrimethylammonium bromide; SDS = sodium dodecyl sulfate; BC= bicontinuous; O/W = oil in water.

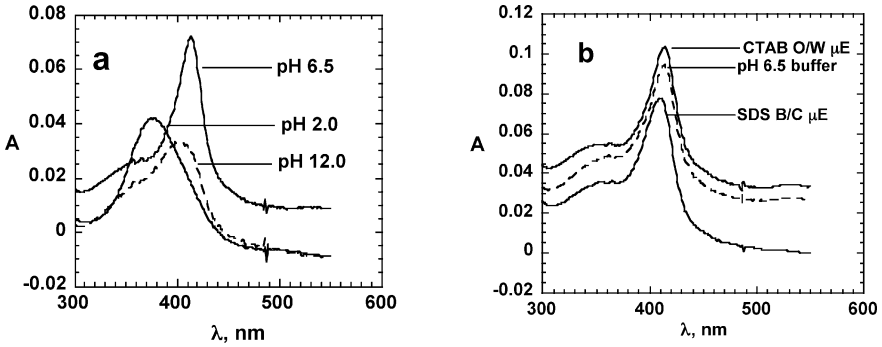

Figure 1. Absorption spectra of Mb/PLL films on fused silica slides: (a) in aqueous phosphate buffers at pH 2.0, 6.5, and 12.0 and (b) in CTAB O/W, SDS B/C microemulsions (μEs) and aqueous buffer solution at neutral pH.

and especially water phase acidity, can be used to control reaction kinetics.

Experimental Section

Chemicals, Solutions, and Microemulsions. Poly-L-lysine (PLL, MW 150 000−300 000) and horse heart myoglobin (Mb) were from Sigma. Mb in acetate buffer, pH 5.5, was filtered through a YM30 filter (Amicon, 30 000 MW cutoff) to give 3.0 mg mL^{-1} Mb.[30] Dodecane, pentanol, 1-butanol, hexadecane, *tert*-butylhydroperoxide, 1-[3-(dimethylamino)propyl]-3-ethylcarbodiimide hydrochloride (EDC·HCl), cetyltrimethylammonium bromide (CTAB), and sodium dodecyl sulfate (SDS) were from Aldrich. Tetradecane was from Acros. The 10 mM phosphate buffer, pH 6.5, included 0.1 M NaCl. Micellar solutions of CTAB (27 mM) and SDS (34 mM) were made in Tris buffer, pH 7.4, containing 50 mM NaCl. Water was purified to specific resistance >15 MΩ cm. Microemulsions were prepared by mixing appropriate weight ratios of components. pH values of water phases were adjusted with hydrochloric acid for pH 2.0 and tetrabutylammonium hydroxide for pH 12.0. The SDS and CTAB microemulsions used (Table 1) were characterized previously.[31,32] All other chemicals were reagent grade.

Voltammetry. A CHI 430 electrochemistry system (CHI Instruments), a saturated calomel electrode (SCE) reference, a platinum (Pt) wire counter, and Mb/PLL-coated pyrolytic graphite (PG) working electrodes were used for voltammetry. A Pine Instruments rotating electrode was used for rotating disk voltammetry (RDV) at a scan rate of 20 mV s^{-1}. Pure nitrogen was purged into solutions for 20 min prior to scans, then maintained over solutions. All experiments were at ambient temperature (22 ± 1 °C). Where slight maxima occurred in RDVs, these were taken as the limiting currents. Reversible cyclic voltammograms were integrated to obtained surface concentrations of protein.

Electrode Film Preparation. Basal plane pyrolytic carbon (PG) disk electrodes ($A = 0.16$ cm^2) were described previously,[8] and were abraded on wet silicon carbide paper (400 grit, Buehler) followed by coarse emery cloth (Crystal Bay 011K). After being rinsed with water, these electrodes were sonicated in water for 30 s, dried, then oxidized electrochemically as described previously.[7,8]

TABLE 2: Visible Soret Absorption Band Positions (nm) for Mb-PLL Films in Microemulsions and Buffers with Water Phases of Different pH

media	neutral pH	basic (pH 12) (nm)	acidic (pH 2) (nm)
SDS BC μE	412	404	405
SDS O/W μE	413	405	400
CTAB B/C μE	413	400	398
CTAB OW μE	412	404	395
buffer	413	400	375

Mb-PLL films were made as described previously.[11] Briefly, 10 μL of freshly prepared 24 mM EDC and 10 μL of 4 mM PLL were deposited on rough, oxidized PG electrodes. After 12 h, electrodes were rinsed with water, then 10 μL of 24 mM EDC and 10 μL of 3 mg mL^{-1} Mb was deposited and reacted for 12 h. A second Mb/PLL bilayer was formed by repeating the above. Frequency changes for films made on quartz crystal microbalance resonators using previously described methods[33] indicated an average film mass of 150 μg cm^{-2} and a nominal film thickness of ~400 nm.

Films were made on fused silica slides for spectroscopy[34] with use of a Hewlett-Packard 8453 UV−vis diode array spectrophotometer for visible absorption and a JASCO 710 spectrometer for circular dichroism (CD). *t*BuOOH water/oil distribution studies were made with use of Quantofix peroxide detection strips, and showed that *t*BuOOH was partitioned almost entirely into water.

Results

Spectra of Mb/PLL Films. Figure 1 shows absorption bands of Mb-PLL films in buffer and in different microemulsions. At neutral pH, native Mb has a characteristic iron heme Soret absorption band at $\lambda_{max} = 409$ nm,[35] and in films this band is several nm higher.[36] In all the microemulsions with neutral water phases, band positions were within experimental error of the native Mb Soret bands (Table 2),[34,36] unlike Mb dissolved in microemulsions which shows 10−20 nm blue shifts.[10] At pH 12 and 2, blue shifts of 7−17 nm were found for the films in microemulsions, less than the 12−38 nm blue shifts in buffers of the same pH (Table 2). Thus, the microemulsions moderate the influence of strong acid and basic water phases on Mb conformation in the films. However, these results do suggest

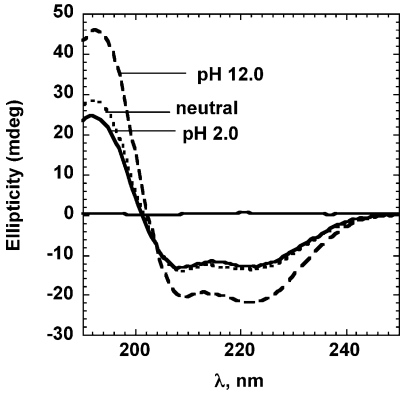

Figure 2. Circular dichroism spectra of Mb/PLL films on fused silica slides in SDS bicontinuous microemulsions with water phases at pH 2.0, neutral, and pH 12.0. Backgrounds from control PLL films without Mb were featureless, and were subtracted from the Mb spectra.

small conformational changes of Mb in the PLL films in fluids with pH 2 and 12 water phases, as also found for Mb in lipid films.[37,38] All Soret band shifts were reversed once the films were returned to neutral pH.

Circular dichroism spectroscopy (CD) was used to monitor the secondary structure of myoglobin in the Mb/PLL films after exposure to microemulsions. CD in the UV region is sensitive to changes in the conformation of the polypeptide backbone. Figure 2 shows the CD spectra of Mb/PLL films in microemulsions and Figure S1 (Supporting Information) shows similar spectra in phosphate buffer solutions with double minima at 222 and 210 nm and a maximum at 193 nm. These spectra are characteristic of the 76% α-helical conformation of native Mb secondary structures.[39] CD results suggested that no gross changes occur in the polypeptide backbone conformation when the films are exposed to microemulsions or to acid or basic media, as also found for films of Mb and polystyrene sulfonate in surfactant-free buffers.[34]

Visible absorption spectra of Mb/PLL films were also observed after addition of 1 mM or greater *t*BuOOH. For Mb in solution, the Soret band at 408 nm shifted to 421 nm on *t*BuOOH addition. Smaller peaks at 503 and 630 nm decreased and were replaced by peaks at 549 nm and a broad peak at ∼580 nm. These observations in buffer solutions are characteristic of conversion of the ferric protein to ferryloxy species.[18] While similar species form in weakly acidic solution,[18,40] they rapidly decompose making observation of their spectra at room temperature difficult. For Mb-PLL films, no new bands were found upon addition of 1 mM *t*BuOOH to buffers or microemulsions. The only observation was a very slow decrease of the Soret band, which may result from slow protein degradation or peroxide-assisted degradation of the film itself, which was not covalently linked to the fused silica slides.

Stability of Mb/PLL Films. Earlier work showed that Mb/PLL films covalently attached to graphite electrodes were stable for more than 8 h of continual voltammetric scanning in microemulsions, even in the presence of mM levels of hydrogen peroxide.[11] Under hydrodynamic conditions (2000 rpm) in microemulsions and pH 6.5 buffer, Mb/PLL films were stable for more than 12 h as monitored by square wave and cyclic voltammetry. The initial scans reached a reproducible steady state after contact with microemulsions for ∼30 min. Stable voltammograms for the protein heme Fe^{III}/Fe^{II} redox couple (Figure 3, 0 mM *t*BuOOH) were observed in all neutral media over 12 h storage in microemulsions with no detectable loss of Mb from the films. Peak potentials did not change except for a small positive shift (∼20 mV) in the CTAB microemulsion. Mb-PLL films in acidic or basic microemulsions showed no loss in voltammetric peak current over several hours under hydrodynamic conditions, but were less stable than in neutral microemulsion over longer periods. Under catalytic conditions in the presence of *t*BuOOH at concentrations used for rotating disk voltammetry (RDV), films remained stable for 3-4 h. Thus, extensive exposure to the peroxide in the acidic and basic media had to be avoided in the catalytic studies.

Cyclic voltammetry (CV) was used to survey the direct electrochemistry of the Mb-PLL films and to obtain surface concentrations of Mb. Symmetric, reversible reduction−oxidation peak pairs for the heme Fe^{III}/Fe^{II} redox couple of Mb in the films were observed in all media studied (for examples see Figures 3 and 4, 0 mM *t*BuOOH, and Figures S2, S3, and S4 in the Supporting Information). Integrations of low scan rate CVs in the different media gave average surface concentrations (±10%) in nmol cm^{-2} as follows: SDS BC (0.20), SDS OW (0.22), CTAB BC (0.33), CTAB OW (0.35), buffer (0.12), SDS micelles (0.13), and CTAB micelles (0.14). Voltammetry results were consistent with nonideal, reversible, thin protein film voltammetry[41] up to scan rates of 1 V s^{-1}. Table 3 shows the formal redox potentials estimated as midpoint potentials between the oxidation−reduction peaks. Small differences in formal redox potentials with changes in media with neutral water phases are most likely due to different interactions between the protein and the fluid components. The effect of pH on the formal potentials is stronger than the effect of microemulsion or surfactant type. In all media, formal potentials shifted significantly positive in going from pH 12.0, to neutral, to pH 2.0

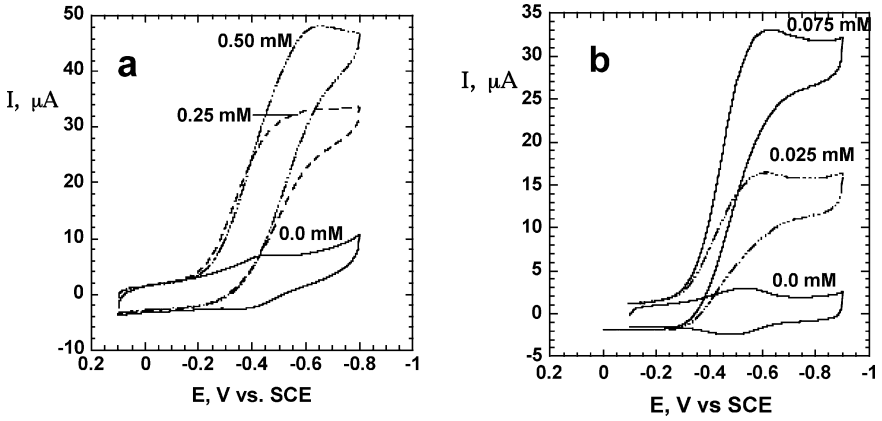

Figure 3. RDVs for *t*BuOOH reduction by the Mb/PLL films at 1000 rpm: (a) in bicontinuous CTAB microemulsion with neutral water phase and (b) in SDS bicontinuous microemulsions with pH 12 water phase. Labels on curves indicate *t*BuOOH concentrations.

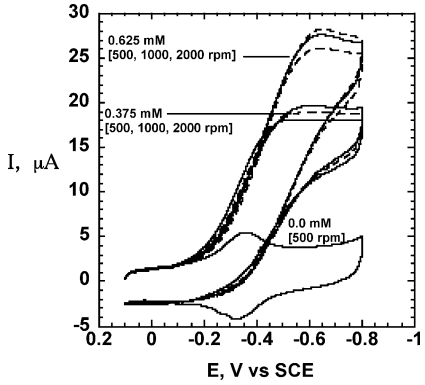

Figure 4. RDV of Mb/PLL films in bicontinuous CTAB microemulsion at neutral pH at different rotation rates for several concentrations of *t*BuOOH labeled on curves.

TABLE 3: Formal Redox Potentials for the Mb/PLL Films at Acidic, Neutral, and Basic Conditions in Microemulsions (μEs) and Buffer Solutions

	E, V vs SCE		
medium	acidic (pH 2.0)	neutral	basic (pH 12.0)
SDS B/C μE	-0.18 ± 0.01	-0.39 ± 0.01	-0.59 ± 0.01
SDS O/W μE	-0.16 ± 0.01	-0.39 ± 0.01	-0.55 ± 0.02
SDS micellar	-0.20 ± 0.02	-0.31 ± 0.01	-0.47 ± 0.02
CTAB B/C μE	-0.19 ± 0.01	-0.38 ± 0.01	-0.60 ± 0.01
CTAB O/W μE	-0.22 ± 0.01	-0.37 ± 0.01	-0.60 ± 0.01
CTAB micellar	-0.22 ± 0.02	-0.34 ± 0.02	-0.52 ± 0.02
aqueous buffer	-0.24 ± 0.01	-0.30 ± 0.01	-0.52 ± 0.01

(Table 3), consistent with proton coupled electron transfer as reported previously for Mb in lipid and polyion films in buffer solutions.[34,42,43]

Catalytic Rotating Disk Voltammetry. Rotating disk voltammetry (RDV) was used to investigate the catalytic reduction of *t*BuOOH by the Mb/PLL films. RDV controls reactant mass transport to achieve steady-state limiting currents related to the Mb turnover rate, and was used to obtain kinetic parameters for the reaction. Catalytic reactions involving an electroactive enzyme film on an electrode are characterized by interfacial electron exchange, enzyme kinetics, and substrate mass transport.[44,45] Under steady-state conditions, the RDV limiting current is given by:

$$\frac{1}{I_{\text{lim}}} = \frac{1}{I_{\text{Lev}}} + \frac{1}{I_{\text{E}}} + \frac{1}{I_{\text{cat}}} \tag{1}$$

where I_{lim} is the limiting current, I_{E} is the exchange current due to interfacial electron transfer between the electrode and primary electron entry/exit site on the enzyme, I_{cat} is the catalytic current characteristic of the enzyme reaction, and I_{Lev} is the Levich current for the transport of substrate between the bulk solution and the enzyme film. Assuming that electron transfer is not limiting at high overpotential, eq 1 becomes

$$\frac{1}{I_{\text{lim}}} = \frac{1}{I_{\text{Lev}}} + \frac{1}{I_{\text{cat}}} \tag{2}$$

Michaelis−Menten enzyme catalysis holds that the substrate initially binds to the enzyme to form a complex, which then is transformed to product(s).[13,46] Scheme 1 illustrates this model for reduction of substrate (S) *t*BuOOH by the Mb/PLL film.

SCHEME 1

$$E_{red} + S \underset{k_{-1}}{\overset{k_1}{\leftrightarrow}} E_{red}S \xrightarrow{k_{cat}} E_{ox} + P$$

Ferric Mb (E_{red}) reacts with *t*BuOOH to give the protein−substrate complex ($E_{red}S$), which reacts to regenerate Mb (E_{ox}) in an oxidized form. If the electrochemistry of E_{ox} in the film is reversible and regenerates E_{red}, a catalytic current that can be used to measure reaction kinetics results from the electrochemical reduction of E_{ox} in the film. The catalytic current I_{cat} is given by the electrochemical Michaels−Menten equation[44,45]

$$I_{\text{cat}} = \frac{nFA\Gamma k_{\text{cat}} C_{\text{s}}}{C_{\text{s}} + K_{\text{m}}} \tag{3}$$

where n is the number of electrons in the electrochemical reaction, C_s is concentration of substrate in solution, Γ is the surface concentration of enzyme in the film (mol cm^{-2}), A is the electrode area (cm^2), F is Faraday's constant, k_{cat} is the catalytic rate constant (s^{-1}), and K_m is the Michaelis dissociation constant given by:

$$K_{\text{m}} = \frac{k_{-1} + k_{\text{cat}}}{k_1} = \frac{[\text{E}_{\text{red}}][\text{S}]}{[\text{E}_{\text{red}}\text{S}]} \tag{4}$$

The ratio k_{cat}/K_m has units of a second-order rate constant (M^{-1} s^{-1}) and provides a direct measure of catalytic efficiency.

Equation 5 is obtained from eq 2 as a form of the Koutecky−Levich equation:

$$\frac{1}{I_{\text{lim}}} = \frac{1}{I_{\text{cat}}} + \left[\frac{1}{0.62nFAD^{2/3}C_{\text{s}}\upsilon^{-1/6}\omega^{1/2}}\right] \tag{5}$$

where υ is the kinematic viscosity of the solution (cm^2 s^{-1}), D is the diffusion coefficient of substrate (cm^2 s^{-1}), and ω is the electrode rotation rate (rad s^{-1}). This equation shows that a plot of $1/I_{lim}$ versus $\omega^{-1/2}$ gives $1/I_{cat}$ as the Y-intercept at infinite rotation rate. I_{cat} vs C_s data obtained in this way can be fit with the model in eq 3 to obtain k_{cat} and K_m. In practice, the best convergence by nonlinear regression is obtained by using the following rearranged version[39b] of eq 3:

$$I_{\text{cat}} = \frac{nFA\Gamma(k_{\text{cat}}/K_{\text{m}})C_{\text{s}}}{(1/K_{\text{m}})C_{\text{s}} + 1} \tag{6}$$

with fitting parameters $m_1 = nFA\Gamma(k_{cat}/K_m)$ and $m_2 = 1/K_m$.

A simpler electrochemical−chemical catalytic (EC′) model was also tested. In this model there is no intermediate $E_{red}S$ complex, only reaction of E_{red} and S to give E_{ox} and products. Then, the catalytic current is linearly related to C_s:[47]

$$I_{\text{cat}} = \left(\frac{F}{RT}\right)k_{\text{cat}}\Gamma C_{\text{s}} \tag{7}$$

where the k_{cat} here is the catalytic rate constant for reaction of E_{red} and S.

Figure 3 shows rotating disk voltammograms of Mb/PLL films in CTAB and SDS microemulsions. Addition of submillimolar *t*BuOOH to the fluid produced a sigmoidal reduction wave larger than the original peak for Mb, accompanied by disappearance of the oxidation peak. The limiting current increased with increasing *t*BuOOH concentration. These data are characteristic of a catalytic reduction of the substrate by the protein film.[47] There was no observable response for *t*BuOOH on PLL/EDC films over the potential range studied in any of the fluids. Addition of catalase to the solutions to scavenge trace hydrogen peroxide did not influence the limiting currents, suggesting the absence of significant hydrogen peroxide in the *t*BuOOH.

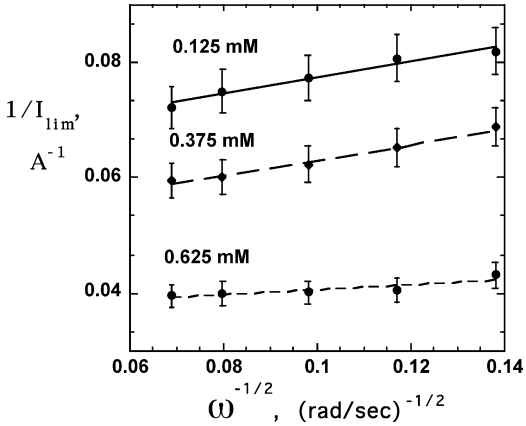

Figure 5. Koutecky−Levich plots (eq 5) showing the influence of rotation rate on I_{lim} for *t*BuOOH reduction on Mb/PLL films in CTAB B/C microemulsions with neutral water phases.

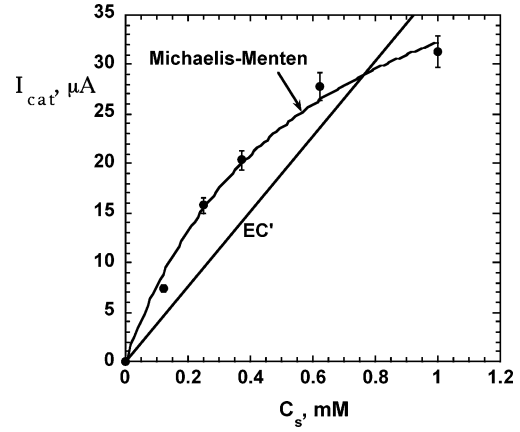

Figure 6. Nonlinear regression fits of Michaelis−Menten (eq 6) and EC′ (eq 7) models (solid lines) to I_{cat} versus *t*BuOOH concentration data (●) for Mb/PLL films in CTAB B/C microemulsions with neutral water phases.

Changes in limiting current with rotation rate are illustrated in Figure 4. Following the Koutecky−Levich equation, catalytic currents, I_{cat}, were obtained from intercepts of plots of $1/I_{lim}$ vs $\omega^{-1/2}$ for different values of C_s (Figure 5). Regression of the I_{cat} vs C_s data sets onto eq 6 provided good fits (Figure 6) from which kinetic parameters were extracted. The linear EC′ model did not fit any of these data sets.

Table 4 shows the kinetic parameters obtained. The aqueous buffer gave the largest values of k_{cat} and k_{cat}/K_m. CTAB and SDS microemulsions gave roughly similar values to each other for k_{cat} and k_{cat}/K_m. Micellar solutions gave slightly larger values for k_{cat} than microemulsions, but similar values of k_{cat}/K_m.

TABLE 4: Michaelis Parameters k_{cat}, K_m, and k_{cat}/K_m from RDV of *t*BuOOH Reduction by PLL/Mb Films from Rotation Rate Dependence (500 to 2000 rpm) in Fluids with Neutral pH Water Phases

media	k_{cat} (s^{-1})	K_m (mM)	$10^{-4}k_{cat}/K_m$ ($M^{-1}s^{-1}$)
SDS B/C	5.6 ± 0.3	0.50 ± 0.01	1.1 ± 0.1
SDS O/W	8.2 ± 0.5	0.80 ± 0.05	1.0 ± 0.01
SDS micellar solution	8.2 ± 1.0	1.2 ± 0.3	0.68 ± 0.03
CTAB B/C	3.8 ± 0.4	0.58 ± 0.11	0.66 ± 0.04
CTAB O/W	4.0 ± 0.8	0.53 ± 0.09	0.75 ± 0.04
CTAB micellar solution	10.5 ± 0.8	0.90 ± 0.1	1.20 ± 0.05
phosphate buffer, pH 6.5	11.5 ± 1.5	0.11 ± 0.01	10.0 ± 0.4

Slow deceases of the limiting currents under catalytic hydrodynamic conditions in fluids with acidic or basic water phases precluded doing a full range of concentration and rotation rate studies in these media on single electrodes. However, stability was sufficient to obtain reproducible data for scans for a series of C_s at a single rotation rate. Since the dependence of the limiting current, I_{lim}, on rate of rotation, ω, was weak (Figure 4), we reasoned that fitting the I_{lim} versus C_s to eq 3 using I_{lim} as an approximation to I_{cat} would provide apparent kinetic constants suitable for comparing the influence of the different fluids in a self-consistent manner. First we confirmed that stability of the films in acidic or basic microemulsions was sufficient to obtain a full concentration dependence at one rotation rate without significant signal deterioration. Next, we compared parameters obtained for the neutral pH fluids in this approximate way (Table S1, Supporting Information) with those obtained from the full [C_s, ω] dependence (Table 4). I_{lim} vs C_s for all the fluids gave very good fits to the Michaelis−Menten equation (Figure 7). The actual values of k_{cat}, K_m, and k_{cat}/K_m differed (~20−50%) from those in Table 4, but very similar trends were observed for the influence of fluid composition. For example, aqueous buffers and CTAB micelles gave the largest values of k_{cat} and aqueous buffer gave the smallest K_m in the approximate and complete methods. The buffer gave largest values of k_{cat}/K_m for both methods, while CTAB microemulsions gave the smallest values. Thus, these data provided confidence that the approximate approach could be used for general comparisons of the influence of fluids with neutral, acidic, and basic water phases on the kinetics.

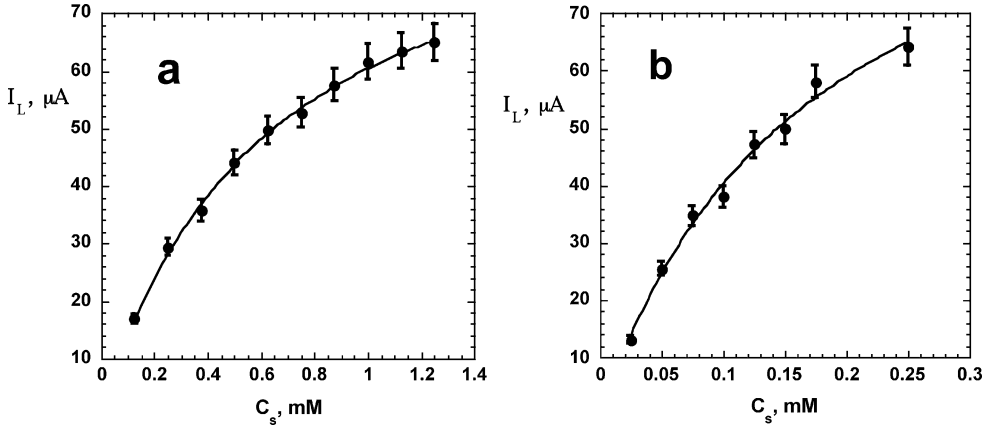

Figure 7. Influence of *t*BuOOH concentration on I_{lim} at 1000 rpm (solid points, as approximations to I_{cat}) for Mb/PLL films fit onto eq 6 (solid lines) by nonlinear regression for data obtained (a) in CTAB bicontinuous microemulsion with neutral water phase and (b) in SDS BC microemulsion with pH 12 with water phase.

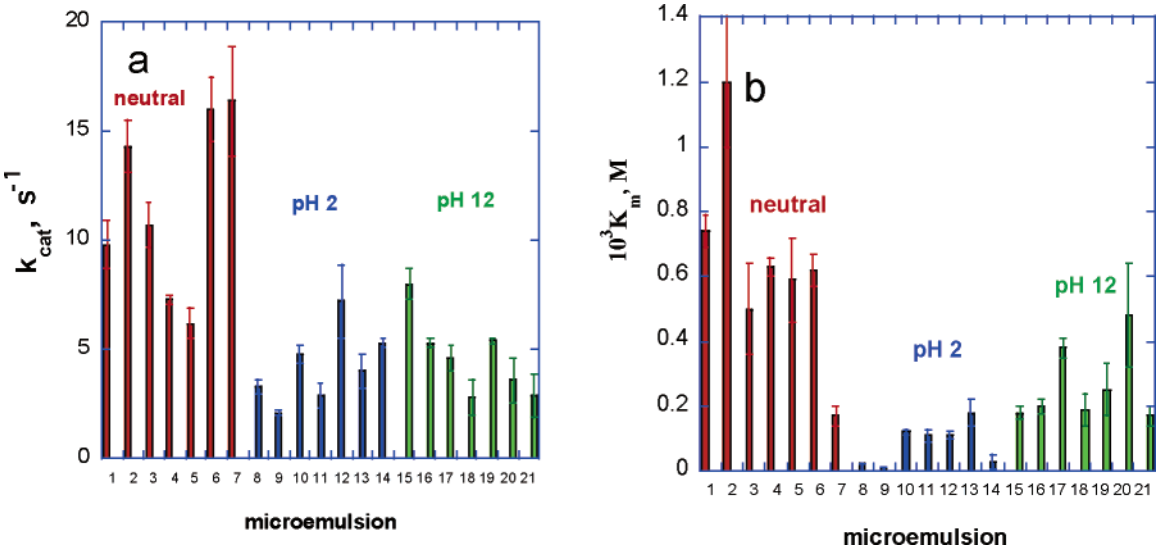

Figure 8. Apparent Michaelis kinetic parameters for reduction of *t*BuOOH by Mb/PLL films in the following microemulsions (cf. Table 1): (1) SDS B/C, (2) SDS O/W, (3) SDS micelles, (4) CTAB B/C, (5) CTAB O/W, (6) CTAB micelles, (7) pH 6.5 buffer, (8−14) same as 1−7 except the water phase was pH 2, and (15−21) same as 1−7 except the water phase was pH 12.

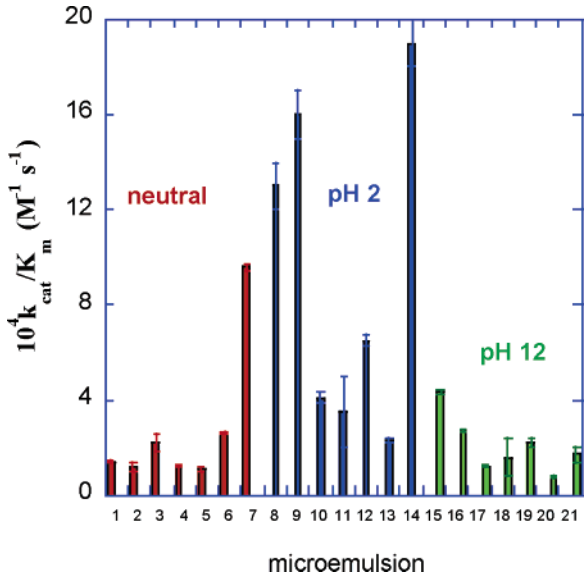

Figure 9. Apparent Michaelis ratio k_{cat}/K_m for reduction of *t*BuOOH by Mb/PLL films in the following microemulsions (cf. Table 1): (1) SDS B/C, (2) SDS O/W, (3) SDS micelles, (4) CTAB B/C, (5) CTAB O/W, (6) CTAB micelles, (7) pH 6.5 buffer, (8−14) same as 1−7 except the water phase was pH 2, and (15−21) same as 1−7 except the water phase was pH 12.

Bar charts of k_{cat} and K_m (Figure 8) reveal the influence of the different fluids on reaction kinetics. First, water phase acidity had a larger influence than microemulsion or surfactant type. The fluids with neutral water phases had the largest values of k_{cat} and K_m. Values of k_{cat} were roughly similar to each other for fluids with pH 2 and 12 water phases. It is also notable that the neutral SDS W/O microemulsion, CTAB micelles, and the pH 6.5 buffer had the largest values of k_{cat}. The acidic fluids had the smallest values of K_m.

Comparing the apparent k_{cat}/K_m ratios in the same format (Figure 9), the values from acidic water phase media are the largest. Media with neutral or pH 12 water phases gave smaller k_{cat}/K_m, with similar values for the two acidities. The SDS microemulsions with pH 2 water phases and the pH 2 and 6.5 buffers stand out as having the largest k_{cat}/K_m values.

Discussion

Results presented above show that the generation of ferryloxy myoglobin species in Mb/PLL films by *t*BuOOH as measured from analysis of I_{cat} vs C_s from RDV in neutral media is consistent with Michaelis−Menten kinetics (Figure 6) in microemulsions, aqueous buffers, and micellar solutions. In addition, I_{lim} vs C_s at fixed rotation rate in all media also fit the Michaelis−Menten model (Figure 7), allowing comparisons of the reaction in fluids with acidic, neutral, and basic water phases. Scheme 2 illustrates an oversimplified pathway for the reaction

SCHEME 2

$$MbFe^{III} + tBuOOH \leftrightarrow [MbFe^{III}tBuOOH] \quad (K_m) \qquad (8)$$

$$[MbFe^{III}\text{-}tBuOOH] \rightarrow \bullet MbFe^{IV}{=}O + tBuOH \quad (k_{cat}) \qquad (9)$$

$$\bullet MbFe^{IV}{=}O + 2e^- + 2H^+ \rightarrow MbFe^{III} + H_2O \quad \text{(at electrode)} \qquad (10)$$

based on the prevalent (67%) heterolytic *t*BuOOH cleavage mechanism for reaction with metmyoglobin. Reaction of the ferric enzyme with *t*BuOOH gives the protein−substrate complex (eq 8), which then undergoes an internal redox reaction with rate constant k_{cat} to yield the Mb ferryloxy radical and *tert*-butyl alcohol (eq 9). While we did not observe spectroscopic signatures of the ferryloxy species in Mb/PLL films, RDV catalytic currents in the presence of *t*BuOOH as well as the ability of Mb/PLL films to support peroxide-initiated styrene epoxidation[11,12] provide clear evidence for its generation. Reduction of $\bullet MbFe^{IV}{=}O$ at the electrode regenerates $MbFe^{III}$ (eq 10). An analogous route can be envisioned for the less prevalent homolytic peroxide cleavage pathway (33%) where nonradical $MbFe^{IV}{=}O$ and *tert*-butyloxy radical are formed,[28,29] which may then be reduced at the electrode. These two pathways cannot be distinguished by the RDV results.

Regardless of exact mechanistic details, analysis of RDV limiting currents with the electrochemical Michaelis−Menten model provided a self-consistent approach to examine the influence of microemulsions on the apparent reaction kinetics. Water phase acidity−basicity had a much greater influence on kinetic parameters (Figures 8 and 9) than microemulsion or surfactant type. Values of k_{cat} and K_m were largest for systems with neutral water phases, then next largest for pH 12, and

smallest for at pH 2 water phases. SDS W/O microemulsion, CTAB micelles, and pH 6.5 buffer had the largest values of k_{cat}. The smallest values of K_m were found in the fluids with pH 2 water phases.

To interpret these kinetic differences, we first recall that spectral data reported in this paper and previously[11] suggest that Mb in polyion films resides in a water-rich environment. This view is supported here by visible absorbance and CD spectra of the Mb/PLL films (Figures 1 and 2, Table 2) that suggest near native conformation for Mb within films in neutral microemulsions. Soret band positions (Table 2) and CD spectra were nearly identical with that in pH 6.5 buffer in all the neutral surfactant-based fluids. Soret bands are expected to shift blue if Mb resided in oil-rich environments.[10] The native state of metmyoglobin ($MbFe^{III}$) features a proximal histidine bound to iron below the plane of the heme, and a distal histidine hydrogen bonded to ligated water above the heme.[48] This high-spin $MbFe^{III}-H_2O$ species predominates in solution between pH 5.5 and 8.[49] Mb in solution partially unfolds beginning at pH <5, and the Soret band is broadened and blue shifted.[50] At pH 3 the Soret maximum for dissolved, partly unfolded myoglobin is 375 nm. An axial water proton dissociates from $MbFe^{III}-H_2O$ with $pK_a \sim 8.3$,[42] and low spin $MbFe^{III}-OH$ predominates in solution at pH >9.[50] This proton dissociation decreases Soret absorbance, as also seen in Figure 1a (pH 12), but does not significantly influence the band position. Thus, the 8−12 nm blue shift for Mb/PLL in the pH 12 media (Table 2) may reflect both dissociation of water to give $MbFe^{III}-OH$ and small conformational changes around the iron heme. In general, the Soret band positions of the films (Table 2) suggest conformational differences from the native configuration around the heme group in media with pH 2 and 12 water phases. These Soret band shifts while the UV CD spectra remain characteristic of helical polypeptide backbone conformation similar to native Mb support the view that conformation changes are mainly in the iron heme region.

Since eq 9 reflects an internal redox reaction of the protein with bound *t*BuOOH, we might expect that k_{cat} would increase as the $MbFe^{III}$ formal potential becomes more negative based on linear free energy predictions.[47] Within the neutral fluid data set (Table 4), where film protein conformations are the same in all fluids, there is an imperfect correlation of k_{cat} with formal potential (Table 3). The standard potential of the film in the pH 6.5 buffer is the most negative for this data set, and also gave the largest k_{cat} for the neutral systems. Further inspection of Table 3 shows that the formal potential of $MbFe^{III}$ in the films becomes more negative in going from pH 2 to neutral to pH 12, consistent with protein-coupled electron transfer reported for Mb in lipid and polystyrene sulfonate films.[34,42] Formal potential difference between pH 2 and neutral is smallest in buffer, and larger in microemulsions, suggesting that there may be a diminished pH dependence of formal potential in acidic buffers as seen for lipid films of Mb.[37] Additional studies are needed to investigate such phenomena further.

In any case, k_{cat} is largest in fluids with neutral water phases, next largest at pH 12, and smallest for pH 2 systems. Thus, there is no correlation of k_{cat} with the pH-controlled formal potentials. The most likely reason is that each protein conformation in the heme region is different at each of the three different acidities of the water environment around the protein, as supported by Soret band positions (Table 2). In acidic media, Soret blue shifts of 7−17 nm at pH 2 and 7−12 nm at pH 12 (Table 2) suggest various levels of unfolding near the heme group, suggesting that in each case the distance of electron (or oxygen) transfer may differ within the $E_{red}S$ complexes and this may have a profound effect on k_{cat}. In other words, the reactant protein in fluids of different water phase acidities has a significantly different conformation, which may bind and react differently with *t*BuOOH in an inner sphere-like process. A stable form of partially denatured *molten globule* Mb exists in solution around pH 3.5−5 and has ∼45% α-helix[48] as opposed to 76% α-helix for the native form. However, CD spectra of the films (cf. Figure 2) suggest that major helix unfolding does not occur in the films at pH 2 or 12, while Soret band positions indicate that conformation changes near the iron heme in acid and basic environments (Table 2). Consequently, the pH 2 and 12 media give smaller k_{cat} values than fluids featuring the neutral water phases. Thus, we rationalize that conformational changes governed by the acidity of the water environment around ferric Mb are controlled by water phase acidity, which in turn controls k_{cat}.

Compatible with this reasoning, values of K_m should also be controlled by local conformations near the ferric Mb. Conformations in the acidic and basic film environments achieve stronger binding within the protein−substrate complex and make K_m smaller. The consequences of these differences are seen in Figure 9, showing that ratios of k_{cat}/K_m are largest for the acidic water phase media. Fluids with neutral and basic water phases gave comparable k_{cat}/K_m values, although the neutral buffer approaches values for media with acidic water phases. Thus, gains in k_{cat} achieved in neutral water phases are offset by weaker binding of the protein−substrate complex that compromises the efficiency of the overall reaction. From a practical point of view, acidic SDS microemulsions and pH 2 buffer provide the largest k_{cat}/K_m and the most efficient reaction conditions. However, for reactions of the generated ferryloxy radicals with nonpolar reactants such as styrene, microemulsions have a reactant solubilizing advantage that greatly increases the protein turnover rate,[11] so that acidic SDS microemulsions would be the media of choice.

We can speculate about molecular events involved in ferryloxy radical formation in the film. Polyion−protein films are known to contain considerable amounts of water,[51] and as mentioned above Mb resides in an aqueous environment in the film. Oil/water distribution studies suggest that *t*BuOOH resides almost exclusively in the water phase. Thus, Scheme 2 most likely occurs entirely in an aqueous environment surrounding Mb in the film. We can envision a dynamic water network consistent with the dynamic nature of microemulsion structure allowing delivery of reactant from the water phase of the microemuslions to the reaction sites in the film. While the RDV approach uncouples mass transport in solution from reaction kinetics, it does not explicitly consider in-film dynamics or in-film reactant concentrations at the reaction site that differ from those in solution.[47] Thus, the dependence on water phase dynamics for reactant delivery to Mb within the film may be a reason for the weak dependence of kinetics on microemulsion and surfactant type. As long as there is a reasonable aqueous delivery path for *t*BuOOH to reach Mb in the film, the materials with which the path are constructed are not so important. Clearly the situation is quite complex and detailed molecularly specific studies of reaction environment and molecular dynamics within the film will be needed to further elucidate details.

In summary, Mb/PLL films react with *t*BuOOH to form ferryloxy protein species according to a Michaelis−Menten model. RDV limiting currents analyzed with this model revealed a strong influence of microemulsion water phase acidity on kinetic parameters. Microemulsion and surfactant type had a

smaller influence on reaction kinetics. A large increase in k_{cat} in the fluids with neutral water phases was offset by much weaker binding in the protein−substrate complex. The apparent kinetic constants are likely to be controlled by acidity-controlled protein conformation and its influence on binding of *t*BuOOH in the intermediate protein−substrate complex. Acidic SDS microemulsions and acidic buffer provided the most efficient reaction environment in the film.

Acknowledgment. This work was supported by Grant No. CTS-0335345 from the National Science Foundation (NSF). We thank Dr. Abhay Vaze and Dr. Challa V. Kumar for helpful discussions.

Supporting Information Available: Four additional figures including CD spectra of myoglobin in Mb/PLL films in phosphate buffer solutions with varying pH and cyclic voltammograms of Mb/PLL films in different microemulsions; three tables giving numerical values of apparent kinetic constants from RDV at 1000 rpm in all the fluids studies. This material is available free of charge via the Internet at http://pubs.acs.org.

References and Notes

(1) Rusling, J. F. In *Reactions and Synthesis in Surfactant Systems*; Texter, J., Ed.; Marcel Dekker: New York, 2001; pp 323−335.
(2) Rusling, J. F. In *Encyclopedia of Electrochemistry*; Vol. 2, Interfacial Kinetics and Mass Transport; Calvo, E., Ed.; Marcel Dekker: New York, 2003; pp 418−439.
(3) Rusling, J. F.; Campbell, C. J. In *Encyclopedia of Surface and Colloid Science*; Marcel Dekker: New York, 2002; pp 1754−1770.
(4) Bourrel, M.; Schechter, R. S. *Microemulsions and Related Systems*; Marcel Dekker: New York. 1988.
(5) Ninham, B. W.; Chen, S. J.; Evans, D. F. *J. Phys. Chem.* **1984**, *88*, 5855−5857.
(6) Zhou, D.-L.; Njue, C. K.; Rusling, J. F. *J. Am. Chem. Soc.* **1999**, *121*, 2909−2914.
(7) Campbell, C. J.; Njue, C. K.; Nuthakki, B.; Rusling, J. F. *Langmuir* **2001**, *17*, 3447−3453.
(8) Njue, C. K.; Rusling, J. F. *J. Am. Chem. Soc.* **2000**, *122*, 6459−6463.
(9) Schoemaker, H. E.; Mink, D.; Wubbolts, M. G. *Science* **2003**, *299*, 1694−1697.
(10) Kamau, G. N.; Guto, M. P.; Munge, B.; Panchagnula, V.; Rusling, J. F. *Langmuir* **2003**, *19*, 6976−6981.
(11) Vaze, A.; Parizo, M.; Rusling, J. F. *Langmuir* **2004**, *20*, 10943−10948.
(12) Vaze, A.; Rusling, J. F. *Faraday Discuss.* **2005**, *129*, 265−274.
(13) Matthews, R. C.; van Holde, E. K. *Biochemistry*; Benjamin/Cummings Publishing Co.: New York, 1990.
(14) Ortiz de Montellano, P. R.; Catalano, C. E. *J. Biol. Chem.* **1985**, *260*, 9265−9271.
(15) Rao, S. I.; Wilks, A.; Hamberg, M.; Ortiz de Montellano, P. R. *J. Biol. Chem.* **1994**, *269*, 7210−7216.
(16) Rao, S. I.; Wilks, A.; Ortiz de Montellano, P. R. *J. Biol. Chem.* **1993**, *268*, 803−809.
(17) Kong, J.; Mbindyo, J. N.; Wu, X.; Zhou, J. X.; Rusling, J. F. *Biophys. Chem.* **1999**, *79*, 219−229.
(18) Onuoha, A. C.; Zu, X.; Rusling, J. F. *J. Am. Chem. Soc.* **1997**, *119*, 3979−3986.
(19) Zu, X.; Lu, Z.; Zhang, Z.; Schenkman, J. B.; Rusling, J. F. *Langmuir* **1999**, *15*, 7372−7377.
(20) Yonetoni, T.; Schleyer, H. *J. Biol. Chem.* **1967**, *242*, 1974−1979.
(21) Turner, J. J. O.; Rice-Evans, C. A.; Davies, M. J.; Newman, E. S. R. *Biochem. J.* **1991**, *277*, 833−837.
(22) Choe, Y. S.; Rao, S. I.; Ortiz de Montellano, P. R. *Arch. Biochem. Biophys*. **1994**, *314*, 126−131.
(23) (a) Sitter, A. J.; Reczek, C. M.; Terner, J. *Biochim. Biophys. Acta* **1985**, *828*, 229−235. (b) Chance, M.; Powers, L.; Kumar, C.; Chance, B. *Biochemistry* **1986**, *25*, 1259−1265.
(24) (a) Schulz, C. E.; Chiang, R.; Debrunner, P. G. *J. Phys. Colloq.* **1979**, *40*, 534−536. (b) Foote, N.; Gadsby, P. M. A.; Greenwood, C.; Thomson, A. J. *Biochem. J.* **1989**, *261*, 515−522.
(25) La Mar, G. N.; De Ropp, J. S.; Latos-Grazynski, L.; Balch, A. L.; Johnson, R. B.; Smith, K. M.; Parish, D. W.; Cheng, R.-J. *J. Am. Chem. Soc.* **1985**, *105*, 782−787.
(26) Zhang, Z.; Chouchane, S.; Magliozzo, R. S.; Rusling, J. F. *Anal. Chem*. **2002**, *74*, 163−170.
(27) Allentoff, A. J.; Bolton, J. L.; Wilks, A.; Thompson, J. A.; Ortiz de Montellano, P. R. *J. Am. Chem. Soc.* **1992**, *114*, 9744−9749.
(28) Van der Zee, J. *Biochem. J*. **1997**, *322*, 633−639.
(29) Chen, Y.-R.; Mason, R. P. *Biochem. J.* **2002**, *365*, 461−469.
(30) Nassar, A.-E. F.; Willis, W. S.; Rusling, J. F. *Anal. Chem.* **1995**, *67*, 2386−2392.
(31) Mackay, R. A.; Myers, S. A.; Bodalbhai, L.; Brajter-Toth, A. *Anal. Chem.* **1990**, *62*, 1084−1090.
(32) Myers, S. A.; Mackay, R. A.; Brajter-Toth, A. *Anal. Chem*. **1993**, *65*, 3447−3453.
(33) Zhou, L.; Rusling, J. F. *Anal. Chem*. **2001**, *73*, 4780−4786.
(34) Panchagnula, V.; Kumar, C. V.; Rusling, J. F. *J. Am. Chem. Soc.* **2002**, *124*, 12515−12521.
(35) Puett, D. *J. Biol. Chem.* **1973**, *248*, 4623−4634.
(36) Rusling J. F.; Nassar, A.-E. F. *J. Am. Chem. Soc.* **1993**, *115*, 11891−11897.
(37) Rusling, J. F. *Acc. Chem. Res.* **1998**, *31*, 363−369.
(38) Alcantara, K. E.; Rusling, J. F. *Electrochem. Commun.* **2005**, *7*, 223−226.
(39) (a) Johnson, W. C. *Annu. Rev. Phys. Chem.* **1978**, *29*, 93−114. (b) Rusling, J. F.; Kumosinski, T. F. *Nonlinear Computer Modeling of Chemical and Biochemical Data*; Academic Press: New York, 1996.
(40) (a) King, N. K.; Winfield, M. E. *Aust. J. Biol. Sci.* **1966**, *19*, 211−217. (b) Wittenberg, J. B. *J. Biol. Chem.* **1978**, *253*, 5694−5695. (c) Foote, N.; Gadsby, P. M. A.; Greenwood, C.; Thomson, A. J. *Biochem. J.* **1989**, *261*, 515−522.
(41) Rusling, J. F.; Zhang, Z. In *Handbook Of Surfaces And Interfaces Of Materials*; Vol. 5, Biomolecules, Biointerfaces, and Applications; Nalwa, R. W., Ed.; Academic Press: New York, 2001; pp 33−71.
(42) Nassar, A.-E. F.; Hu, N.; Rusling, J. F.; Kumosinski, T. F. *J. Phys. Chem. B* **1997**, *101*, 2224−2231.
(43) Munge, B.; Estavillo, C.; Schenkman J. B.; Rusling, J. F. *ChemBioChem* **2003**, *4*, 82−89.
(44) Heering, H. A.; Hirst, J.; Armstrong, F. A. *J. Phys. Chem. B* **1998**, *102*, 6889−6902.
(45) Sucheta, A.; Cammack, R.; Weiner, J.; Armstrong, F. A. *Biochemistry* **1993**, *32*, 5455−5465.
(46) Cantor, C. R.; Schimmel, P. R. *Biophysical Chemistry*: *The Behavior of Biological Macromolecules*; W. H. Freeman and Co.: New York, 1980; Part III, pp 892−901.
(47) Andrieux, C. P.; Saveant, J. M. In *Molecular Design of Electrode Surfaces*; Techniques of Chemistry Series, Vol. 22; Murray, R. W., Ed.; Wiley-Interscience: New York, 1992; pp 207−267.
(48) (a) Yang, A.-S.; Honig, B. *J. Mol. Biol.* **1994**, *237*, 602−614. (b) Bashford, D.; Case, D. A.; Dalvit, C.; Tennant, L.; Wright, P. E. *Biochemistry* **1993**, *32*, 8045−8056. (c) Cocco, M. J.; Kao, Y.-H.; Phillips, A. T.; Lecomte, J. T. J. *Biochemistry* **1992**, *31*, 6481−6491.
(49) (a) Goto, Y.; Fink, A. L. *J. Mol. Biol.* **1990**, *214*, 803−805. (b) Stigter, D.; Alonso, D. O. V.; Dill, K. A. *Proc. Natl. Acad. Sci. U.S.A.* **1991**, *88*, 4176−4180.
(50) (a) Theorell, H.; Ehrenberg, A. *Acta Chem. Scand.* **1951**, *5*, 823−848. (b) George, P.; Hanania, G. *Biochem. J.* **1952**, *52*, 517−523. (c) Brunori, M.; Giacometti, G. M.; Antonini, E.; Wyman, J. *J. Mol. Biol.* **1972**, *63*, 139−152.
(51) (a) Lvov, Y. In *Protein Architecture*: *Interfacing Molecular Assemblies and Immobilization Biotechnology*; Lvov, Y., Möhwald, H., Eds.; Marcel Dekker: New York, 2000; pp 125−167. (b) Lvov, Y. In *Handbook Of Surfaces And Interfaces Of Materials*; Nanostructured Materials, Micelles and Colloids, Vol. 3; Nalwa, R. W., Ed.; Academic Press: San Diego, CA, 2001; p. 170−189.